SHORT COMMUNICATION

Irradiation accelerates SARS-CoV-2 infection by enhancing sphingolipid metabolism

Zhuanzhuan Wei | Yiyi Jiang | Gaomei Zhao | Chenwenya Li | Songling Han | Yin Chen | Tao Wang | Tianmin Cheng | Junping Wang | Cheng Wang [ID]

State Key Laboratory of Trauma, Burns and Combined Injury, Chongqing Engineering Research Center for Nanomedicine, Institute of Combined Injury of PLA, College of Preventive Medicine, Third Military Medical University, Chongqing, China

Correspondence
Cheng Wang and Junping Wang, State Key Laboratory of Trauma, Burns and Combined Injury, Chongqing Engineering Research Center for Nanomedicine, Institute of Combined Injury of PLA, College of Preventive Medicine, Third Military Medical University, Chongqing 400038, China.
Email: wangctmmu@126.com and wangjunping@tmmu.edu.cn

Abstract

Cancer patients who receive radiotherapy have a high risk of severe acute respiratory syndrome-coronavirus-2 (SARS-CoV-2) infection, but the concrete reason remains unclear. Herein, we investigated the influence of irradiation on the vulnerability of cancer cells to SARS-CoV-2 using S pseudovirions and probed the underlying mechanism via RNA-seq and other molecular biology techniques. Owing to the enhancement of sphingolipid metabolism, irradiation accelerated pseudovirion infection. Mechanistically, irradiation induced the expression of acid sphingomyelinase (ASM), which catalyses the hydrolysis of sphingomyelin to ceramide, contributing to lipid raft formation and promoting SARS-CoV-2 invasion. Inhibition of lipid raft formation with methyl-β-cyclodextrin (MβCD) or the tyrosine kinase inhibitor genistein and ASM suppression through small interfering RNA or amitriptyline (AMT) treatment abolished the enhancing effect of irradiation on viral infection. Animal experiments supported the finding that irradiation promoted SARS-CoV-2 S pseudovirion infection in A549 cell tumour-bearing BALB/c nude mice, whereas AMT treatment dramatically decreased viral infection. This study discloses the role of sphingolipid metabolism in irradiation-induced SARS-CoV-2 infection, thus providing a potential target for clinical intervention to protect patients receiving radiotherapy from COVID-19.

KEYWORDS
acid sphingomyelinase, amitriptyline, ceramide, irradiation, SARS-CoV-2

1 | INTRODUCTION

Coronavirus disease 2019 (COVID-19) pandemic induced by severe acute respiratory syndrome-coronavirus-2 (SARS-CoV-2), which transmits among humans principally via the contact, droplet, and airborne or aerosol routes,[1] is an ongoing concern worldwide. The association of SARS-CoV-2 spike (S), which is composed of S1 and S2 subunits, with angiotensin-converting enzyme 2 (ACE2) located on sensitive cells such as type 2 alveolar epithelial cells and enterocytes,[2] is the initial step of infection. After adherence, the S protein is cleaved at the S1/S2 boundary by the transmembrane serine protease TMPRSS2, which further mediates viral fusion with the cell membrane.[3] Alternatively, SARS-CoV-2 preferentially enters cells with no or minimal TMPRSS2 expression via endocytosis.[4]

Dynamin-dependent endocytosis pathways, such as caveolin-mediated endocytosis, clathrin-mediated endocytosis, and fast endophilin-mediated endocytosis, and dynamin-independent pathways, including lipid raft pathways and macropinocytosis, have been investigated for their roles in viral entry.[5] A recent study showed that SARS-CoV-2 invaded human embryonic kidney (HEK)-239T cells

highly expressing ACE2 in a manner dependent on lipid rafts,[6] which are the liquid-ordered membranes with abundant cholesterol and sphingolipids. It has been discovered that depletion of cholesterol and consumption of ceramide (CER), which is the backbone of sphingolipids, both decreased SARS-CoV-2 infection.[6,7]

Based on the processes of infection, many inhibitors have been developed to combat SARS-CoV-2.[8] The related research has paved the way for discovery of the underlying causes for the vulnerability of certain populations to the virus. For instance, the increase in ACE2 expression induced by the diabetic milieu explains why diabetic patients are more prone to infection and develop more severe COVID-19 than healthy individuals.[9] Similar to diabetic patients, cancer patients, particularly those who receive radiotherapy, are considered to have high risks of infection and mortality,[10,11] but the concrete reason remains unclear. A recent study revealed that abnormal cell metabolism promotes viral invasion.[9] Irradiation has great impacts on the metabolism of target cells and may affect SARS-CoV-2 invasion.[12] In this study, we confirmed for the first time, that irradiation induced a vulnerable cellular state for SARS-CoV-2.

2 | MATERIALS AND METHODS

2.1 | In vitro SARS-CoV-2 S pseudovirion infection assay

Human nonsmall cell lung cancer A549 cells and colon adenocarcinoma Caco-2 cells were obtained from Chinese Academy of Sciences. The cells were cultured in Dulbecco's modified Eagle's medium (DMEM, HyClone, Thermo Fisher Scientific) containing 10% foetal bovine serum (FBS, Gibco) and seeded into a 96-well plate at a density of 5×10^3 cells per well. After adherence, the cells were exposed to 1, 2, and 4 Gy of γ-ray irradiation at 1 Gy/min. A total of 1×10^6 TU of SARS-CoV-2 S pseudovirions expressing a luciferase reporter (Tsingke Biotechnology) were added after 18 h, followed by a coincubation at 37°C for 6 h. The pseudovirions were then removed, and the cells were cultured for another 48 h. A luciferase reporter assay system (E1910; Promega) was employed to determine pseudovirion infection. These experiments were conducted in triplicate and repeated twice on different days.

2.2 | Immunofluorescence

The cells were seeded on sterile glass slides in a 24-well plate at a density of 1×10^4 cells per well. Irradiation was performed after cell adherence using a 4 Gy γ-ray. A549 cells were exposed to 1×10^6 TU of SARS-CoV-2 S pseudovirions after 18 h, and the coincubation was sustained for 6 h. The antibodies used for S1, acid sphingomyelinase (ASM), and CER detections were shown in Supporting Information: Table S1. A Zeiss LSM 780 NLO confocal microscope was employed to observe the cells.

2.3 | RNA sequencing (RNA-seq)

Total RNA was extracted from the cells in the absence and presence of γ-ray radiation (4 Gy, 1 Gy/min) using TaKaRa RNAiso Plus reagent. Library construction and RNA-seq were carried out by Tsingke Biotechnology as we recently described.[13] Kyoto Encyclopedia of Genes and Genomes (KEGG) analysis was conducted by Phyper.

2.4 | Quantitative real-time polymerase chain reaction (q-PCR)

The RNA from cells and mouse tumours was extracted using TaKaRa RNAiso Plus reagent. Reverse transcription was performed with a TaKaRa PrimeScript RT-PCR kit (RR047A). The primers for ASM, EGFP, and β-actin were shown in Supporting Information: Table S2. The data were recorded using Bio-Rad iQ5 standard edition optical system software (version 2.1). This assay was conducted in duplicate and repeated three times on different days.

2.5 | Western blotting analysis

The cells irradiated with a 4 Gy γ-ray were cultured for 6, 12, 24, and 48 h. After twice washes with sterile PBS, the cells were lysed with RIPA lysis and extraction buffer (P0013C; Beyotime). The antibodies were shown in Supporting Information: Table S3.

2.6 | RNA interference and inhibition assay

Cells were transfected with ASM siRNA (sense, uuaccguguguac-caaauaDCDC; antisense, DCDCaauggcacacaugguuuau) using Lipofectamine 3000 (L3000-015; Invitrogen). The cells were irradiated with a 4 Gy γ-ray after ASM silencing. A total of 1×10^6 TU of SARS-CoV-2 S pseudovirions were then added 18 h after irradiation, followed by a 6 h coincubation. Amitriptyline (25 μM, AMT, HY-B0527A, MCE) was also used to suppress ASM and was added to the cells 4 h before the addition of pseudovirion. For lipid raft inhibition, genistein (150 μM, HY-N0595, MCE) and methyl-β-cyclodextrin (MβCD, 5 mM, HY-101461, MCE) were added 1 h before pseudovirion addition. The cells were then cultured and lysed for detection as mentioned above. The experiments were conducted in triplicate and repeated twice.

2.7 | CER detection

Caco-2 cells collected at 24 h after irradiation were suspended in 0.5 ml of isopropanol: acetonitrile (1:1, v/v) and were sonicated on ice. The supernate (95 μl) obtained via high-speed centrifugation at

12 000 rpm for 10 min was mixed with 5 µl of the interior standard. A 4 µl aliquot of the supernatant was analysed with Waters UPLC I-Class system, which was equipped with a Waters UPLC HSS T3 column. Solutions were eluted at 0.26 ml/min with A (acetonitrile:-water, 6:4, v/v, 0.1% formic acid, 5 mM ammonium acetate) and

B (isopropanol: acetonitrile, 9:1, v/v, 0.1% formic acid, 5 mM ammonium acetate). Counts of the charged particles and the mass-to-charge ratio were determined with Waters XEVO TQ-S Micro tandem quadrupole mass spectrometry. This experiment was repeated three times.
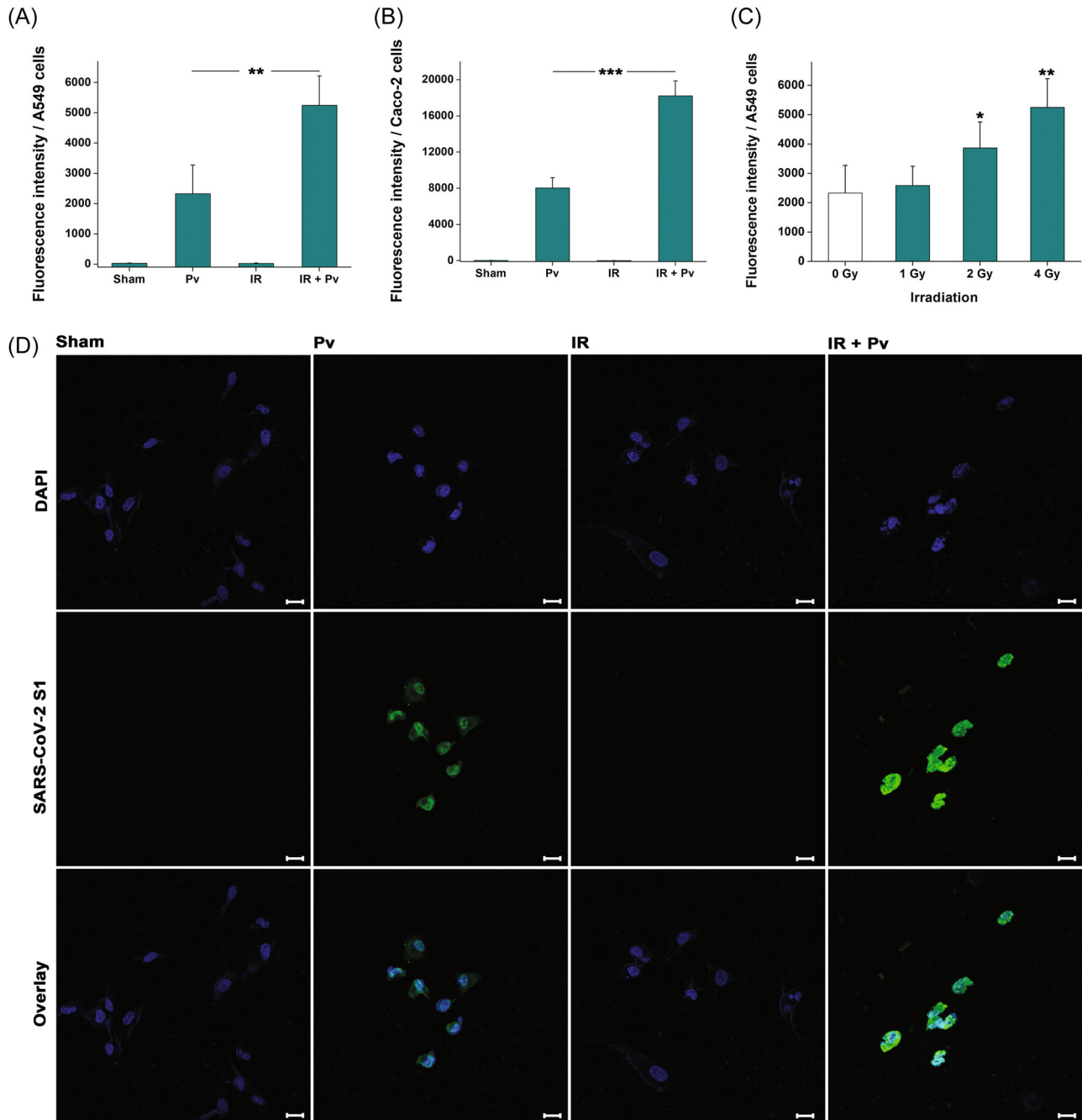
FIGURE 1 Irradiation promotes severe acute respiratory syndrome-coronavirus-2 (SARS-CoV-2) S pseudovirion infection. (A) Shown are pseudovirion infections in A549 and (B) Caco-2 cells in the presence and absence of irradiation treatment. Results are displayed as the mean ± standard deviation (SD). ***$p < 0.001$. (C) Dose-dependent enhancing effect of irradiation on viral infection. Results are shown as the mean ± SD. *$p < 0.05$; **$p < 0.01$. (D) Immunofluorescence microscopy revealing the invasion of SARS-CoV-2 S pseudovirions (green) in A549 cells. Nuclei were stained with DAPI (blue). The scale bar indicates 20 µm.
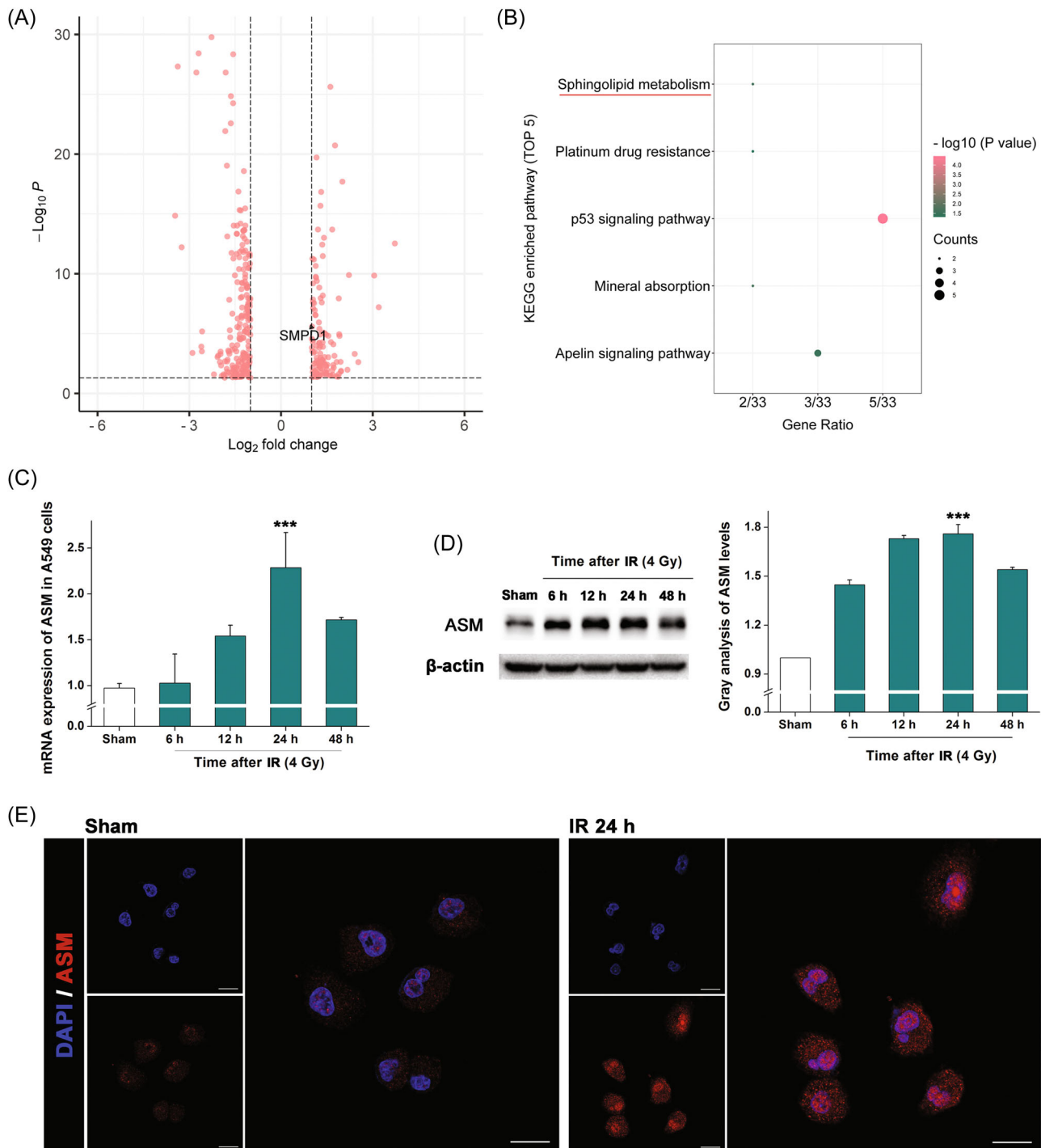
FIGURE 2 Irradiation enhances sphingolipid metabolism by upregulating acid sphingomyelinase (ASM). (A) Volcano figure of the RNA-seq data. Shown are the altered genes in irradiated A549 cells after 24 h. (B) Top five enriched pathways in Kyoto Encyclopedia of Genes and Genomes analysis. (C) Messenger RNA expressions of ASM in irradiated A549 cells at different times. Results are shown as the mean ± SD. ***$p < 0.001$, relative to the sham group. (D) Western blotting analysis revealing the ASM expressions in irradiated A549 cells. β-actin was used as the reference. Histogram shows the results of gray analysis for the protein bands. Results are shown as the mean ± SD. ***$p < 0.001$, relative to the sham group. (E) Immunofluorescence microscopy revealing the expressions of ASM (red) in A549 cells. Nuclei were stained with DAPI (blue). The scale bar indicates 20 μm. SD, standard deviation.

## 2.8 | In vivo SARS-CoV-2 S pseudovirion infection assay

A tumour-bearing model was established as we previously described using BALB/c nude mice (18–22 g).[14] The mice were subcutaneously injected with 2×10^9 CFU of A549 cells in the right hind leg. AMT was intraperitoneally injected at 10 mg/kg twice a day when the tumor volume reached approximately 75 mm³. The tumour sites were locally irradiated with a 4 Gy γ-ray (1 Gy/min) 2 days later. A total of 1×10^7 TU of SARS-CoV-2 S pseudovirions expressing enhanced green fluorescent protein (EGFP, LV-Spike-nCOV, Tsingke Biotechnology) were given through the mouse tail vein at 24 h after irradiation.[2] After 48 h, the mice were killed to obtain the tumour tissues, which were then homogenized and analysed by q-PCR. The animal experiment was approved by the Animal Experimental Ethics Committee of Army Medical University (AMUWEC20226265).

2.9 | Statistical analysis

Statistical analysis was conducted by GraphPad Prism 8 (GraphPad Software Inc.) using the LSD multiple-comparison test. $p < 0.05$ indicated statistical significance.

3 | RESULTS AND DISCUSSION

To investigate the influence of irradiation on COVID-19, we initially employed SARS-CoV-2 S pseudovirions equipped with a luciferase reporter system to infect A549 cells in the absence and presence of a 4 Gy γ-ray irradiation. As shown in Figure 1A, irradiation markedly intensified pseudovirion infection, consistent with the result discovered in Caco-2 cells (Figure 1B). Notably, the enhancing effect occurred in a dose-dependent manner (Figure 1C). Immuno-fluorescence was further conducted by tracing SARS-CoV-2 S1 and
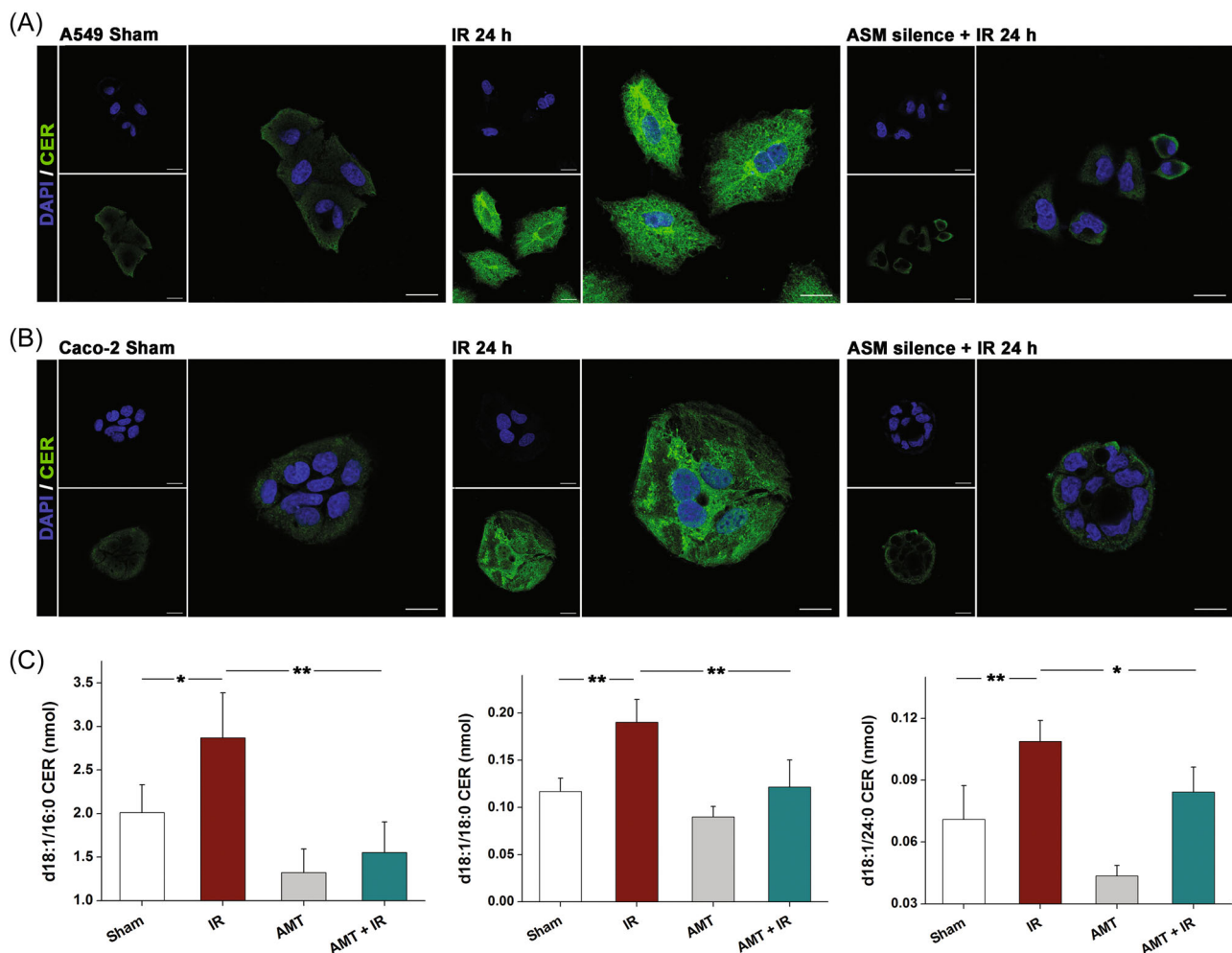

FIGURE 3 Irradiation induces CER accumulation in the cells. (A) Immunofluorescence microscopy revealing the CER (green) in A549 and (B) Caco-2 cells. Nuclei were stained with DAPI (blue). The scale bar indicates 20 µm. (C) CER contents in Caco-2 cells in the presence and absence of irradiation treatment. Results are shown as the mean ± SD. *$p < 0.05$; **$p < 0.01$; ***$p < 0.001$. SD, standard deviation.

the results supported that more pseudovirions entered the cytoplasm of A549 cells after irradiation compared with those in the cells without treatment (Figure 1D).

For insights into the underlying mechanism, we performed a transcriptomic study and found that a total of 351 genes (121 upregulated and 230 downregulated, fold change >2, Figure 2A, Supporting Information: Seq data) were altered in irradiated A549 cells after 24 h. The sphingolipid metabolism was determined to be enriched via KEGG analysis (Figure 2B). The enzyme ASM, which is encoded by the SMPD1 gene in humans and catalyses the hydrolysis of sphingomyelin to CER,[7] was found to be upregulated in the sequencing ($p < 0.001$). Considering the deviation between RNA-seq data and the accurate expression, we performed q-PCR to confirm this result and discovered that the mRNA expression of ASM in

irradiated A549 cells was on average 2.28-fold higher than that in untreated cells after 24 h (Figure 2C, $p < 0.001$). Western blotting analysis showed that ASM was significantly increased after irradiation (Figure 2D, $p < 0.001$), in line with the findings revealed by immunofluorescence (Figure 2E).

ASM alterations were also detected in Caco-2 cells (Supporting Information: Figure S1). A higher ASM upregulation was observed in Caco-2 cells after irradiation than in A549 cells, consistent with the findings that irradiation induced a more severe viral infection in Caco-2 cells than in A549 cells (Figure 1), which indicated that colon adenocarcinoma patients who receive radiotherapy might be more susceptible to COVID-19 than pulmonary adenocarcinoma patients. Clinically, short-term and long-term regimes are widely used in the radiotherapy.[15] Taking colorectal cancer as an example, preoperative
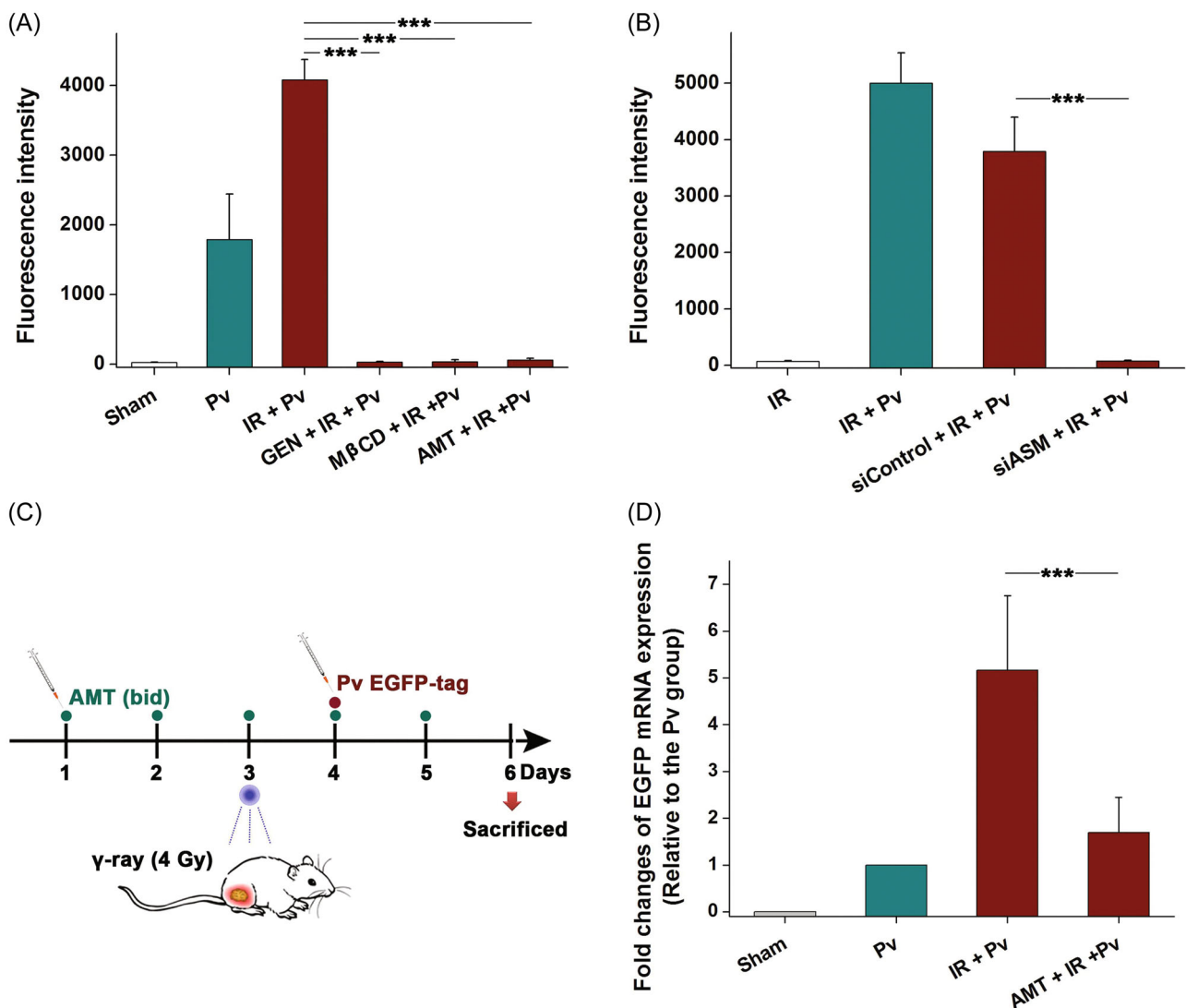
FIGURE 4 Acid sphingomyelinase (ASM) inhibition suppresses SARS-CoV-2 S pseudovirion infection in vitro and in vivo. (A) Shown are pseudovirion infections in A549 cells treated with different kinds of inhibitors. Results are shown as the mean ± SD. ***$p < 0.001$. (B) Inhibition of viral infection by ASM silencing. Results are shown as the mean ± SD. ***$p < 0.001$. (C) Diagram depicting the in vivo SARS-CoV-2 S pseudovirion infection assay. (D) Messenger RNA expressions of enhanced green fluorescent protein in the tumour samples. Results are shown as the mean ± SD. ***$p < 0.001$. SD, standard deviation.

short-term irradiation of 5 Gy × 5 for 1 week is applied before surgery to treat resectable rectal cancer, and long-term irradiation of 1.8 Gy × 28 for 5 weeks is used to downsize locally advanced tumours.[16] As the enhancement of viral infection occurred in a dose-dependent manner, a long-term regimen in which cumulative radiation is delivered in lower doses may be more instrumental than short-term irradiation for avoiding COVID-19.

Upon the alteration of ASM, the levels of downstream product CER, a highly hydrophobic molecule in the outer leaflet of the cell membrane would be changed. We next determined the CER levels in the cells. Immunofluorescence showed that CER was increased in both A549 (Figure 3A) and Caco-2 (Figure 3B) cells at 24 h after irradiation. To decipher the role of ASM in the CER accumulation induced by irradiation, we suppressed ASM expression with siRNA. Along with suppression of ASM (Supporting Information: Figure S2), decreases in CER levels were observed in the irradiated cells. Furthermore, liquid chromatography-mass spectrometry was performed and revealed significantly greater changes in C16 (d18:1/16:0), C18 (d18:1/18:0), and C24 (d18:1/24:0) CER levels in irradiated Caco-2 cells than in cells without irradiation (Figure 3C). Similarly, the increase in CER was abolished by AMT, a tricyclic antidepressant drug that can suppress the action of ASM, suggesting that irradiation induces the expression of ASM, which mediates CER accumulation in cancer cells.

CER molecules can associate with each other spontaneously and generate small CER-enriched membrane domains, changing the biological properties of the cell membrane.[17] It has been discovered the ASM/CER system contributes to membrane protein clustering and lipid raft organization.[18] Our experiment showed that disruption of lipid rafts by cholesterol depletion with 5 mM MβCD significantly decreased pseudovirion infection (Figure 4A, $p < 0.001$). Meanwhile, the tyrosine kinase inhibitor genistein (150 μM), which can suppress lipid raft-mediated endocytosis,[19] markedly attenuated viral infection, suggesting that ASM upregulation might contribute to the enhancing effect of irradiation on cell infection by SARS-CoV-2. Further studies supported that viral infection was reduced after ASM silencing (Figure 4B, $p < 0.001$). Additionally, AMT dramatically decreased viral infection (Figure 4A), suggesting that AMT could be used as a potential inhibitor to reduce the risk of SARS-CoV-2 infection.

The pseudovirion-based mouse infection model as we recently established was then applied to verify this speculation.[2,20] A549 tumour-bearing nude mice were intravenously injected with SARS-CoV-2 S pseudovirions expressing EGFP, and viral infection was measured by detecting EGFP mRNA expression in the tumours using q-PCR (Figure 4C). After local 4 Gy γ-ray irradiation, the EGFP expression level was found to be significantly increased relative to that without irradiation (Figure 4D). Nevertheless, when the mice were treated with 10 mg/kg AMT for 5 days, the enhancing effect of irradiation on viral infection in vivo was notably reduced.

Collectively, the findings of the present study demonstrate an enhancing effect of irradiation on SARS-CoV-2 infection in cancer cells and provide insights into the underlying cellular mechanism. Irradiation upregulates ASM and promotes CER accumulation on the membrane, resulting in intensive lipid raft endocytosis, whereby SARS-CoV-2 enters host cells. Inhibition of ASM with AMT abrogates the influence of irradiation and suppresses viral infection. Like AMT, the functional ASM inhibitors including fluoxetine, fluvoxamine, and maprotiline may have potential applications in the blockade of SARS-CoV-2 infection in patients receiving radiotherapy.[17]

AUTHOR CONTRIBUTIONS

Zhuanzhuan Wei: Investigation; methodology; data curation. **Yiyi Jiang**; Investigation; methodology. **Gaomei Zhao**: Investigation; visualization; **Chenwenya Li**: Formal analysis; validation. **Songling Han**: Visualization; validation. **Yin Chen**: Methodology; formal analysis. **Tao Wang**: Resources; supervision; **Tianmin Cheng**: Funding acquisition; project administration; **Junping Wang**: Funding acquisition; writing – review & editing; supervision. **Cheng Wang**: Conceptualization; funding acquisition; writing – review & editing. Zhuanzhuan Wei, Yiyi Jiang, and Gaomei Zhao contributed equally to this work.

ACKNOWLEDGMENTS

CONFLICT OF INTEREST

The authors declare no conflict of interest.

DATA AVAILABILITY STATEMENT

The data that support the findings of this study are available from the corresponding author upon reasonable request.

ORCID

Cheng Wang http://orcid.org/0000-0002-6690-6433

REFERENCES

1. Priyanka OP, Choudhary OP, Singh I, Patra G. Aerosol transmission of SARS-CoV-2: the unresolved paradox. *Travel Med Infect Dis*. 2020;37:101869. doi:10.1016/j.tmaid.2020.101869
2. Wang C, Wang S, Chen Y, et al. Membrane nanoparticles derived from ACE2-rich cells block SARS-CoV-2 infection. *ACS Nano*. 2021;15(4):6340-6351. doi:10.1021/acsnano.0c06836
3. Hoffmann M, Kleine-Weber H, Schroeder S, et al. SARS-CoV-2 cell entry depends on ACE2 and TMPRSS2 and is blocked by a clinically proven protease inhibitor. *Cell*. 2020;181(2):271-280. doi:10.1016/j.cell.2020.02.052
4. Zhu Y, Feng F, Hu G, et al. A genome-wide CRISPR screen identifies host factors that regulate SARS-CoV-2 entry. *Nat Commun*. 2021;12(1):961. doi:10.1038/s41467-021-21213-4
5. Mercer J, Schelhaas M, Helenius A. Virus entry by endocytosis. *Annu Rev Biochem*. 2010;79(1):803-833. doi:10.1146/annurev-biochem-060208-104626

6. Li X, Zhu W, Fan M, et al. Dependence of SARS-CoV-2 infection on cholesterol-rich lipid raft and endosomal acidification. *Comput Struct Biotechnol J*. 2021;19:1933-1943. doi:10.1016/j.csbj.2021.04.001

7. Carpinteiro A, Edwards MJ, Hoffmann M, et al. Pharmacological inhibition of acid sphingomyelinase prevents uptake of SARS-CoV-2 by epithelial cells. *Cell Rep Med*. 2020;1(8):100142. doi:10.1016/j.xcrm.2020.100142

8. Priyanka OP, Choudhary OP, Singh I. Protective immunity against COVID-19: unravelling the evidences for humoral vs. cellular components. *Travel Med Infect Dis*. 2021;39:101911. doi:10.1016/j.tmaid.2020.101911

9. Garreta E, Prado P, Stanifer ML, et al. A diabetic milieu increases ACE2 expression and cellular susceptibility to SARS-CoV-2 infections in human kidney organoids and patient cells. *Cell Metab*. 2022;34(6):857-873. doi:10.1016/j.cmet.2022.04.009

10. Yu J, Ouyang W, Chua MLK, Xie C. SARS-CoV-2 transmission in patients with cancer at a tertiary care hospital in Wuhan, China. *JAMA Oncol*. 2020;6(7):1108-1110. doi:10.1001/jamaoncol.2020.0980

11. Zorzi M, Guzzinati S, Avossa F, Fedeli U, Calcinotto A, Rugge M. SARS-CoV-2 infection in cancer patients: a population-based study. *Front Oncol*. 2021;11:730131. doi:10.3389/fonc.2021.730131

12. Kalani Roy M, La Carpia F, Cendali F, et al. Irradiation causes alterations of polyamine, purine, and sulfur metabolism in red blood cells and multiple organs. *J Proteome Res*. 2022;21(2):519-534. doi:10.1021/acs.jproteome.1c00912

13. Wang S, Chen Y, Han S, et al. Selenium nanoparticles alleviate ischemia reperfusion injury-induced acute kidney injury by modulating GPx-1/NLRP3/Caspase-1 pathway. *Theranostics*. 2022;12(8):3882-3895. doi:10.7150/thno.70830

14. Chen Y, Shen X, Han S, et al. Irradiation pretreatment enhances the therapeutic efficacy of platelet-membrane-camouflaged antitumor nanoparticles. *J Nanobiotechnology*. 2020;18(1):101. doi:10.1186/s12951-020-00660-z

15. Bentzen SM, Agrawal RK, Aird EG, et al. The UK standardisation of breast radiotherapy (START) trial B of radiotherapy hypofractionation for treatment of early breast cancer: a randomised trial. *Lancet*. 2008;371(9618):1098-1107. doi:10.1016/S0140-6736(08)60348-7

16. Stene C, Polistena A, Gaber A, et al. MMP7 modulation by short- and long-term radiotherapy in patients with rectal cancer. *In Vivo*. 2018;32(1):133-138. doi:10.21873/invivo.11215

17. Kornhuber J, Hoertel N, Gulbins E. The acid sphingomyelinase/ceramide system in COVID-19. *Mol Psychiatry*. 2022;27(1):307-314. doi:10.1038/s41380-021-01309-5

18. Charruyer A, Grazide S, Bezombes C, Müller S, Laurent G, Jaffrézou JP. UV-C light induces raft-associated acid sphingomyelinase and JNK activation and translocation independently on a nuclear signal. *J Biol Chem*. 2005;280(19):19196-19204. doi:10.1074/jbc.M412867200

19. Wang D, Zhou Y, Li X, et al. Mechanisms of pH-sensitivity and cellular internalization of PEOz-b-PLA micelles with varied hydrophilic/hydrophobic ratios and intracellular trafficking routes and fate of the copolymer. *ACS Appl Mater Interfaces*. 2017;9(8):6916-6930. doi:10.1021/acsami.6b16376

20. Wang C, Wang S, Li D, et al. Human cathelicidin inhibits SARS-CoV-2 infection: killing two birds with one stone. *ACS Infect Dis*. 2021;7(6):1545-1554. doi:10.1021/acsinfecdis.1c00096

SUPPORTING INFORMATION

Additional supporting information can be found online in the Supporting Information section at the end of this article.